ISSN 1063-780X, Plasma Physics Reports, 2023, Vol. 49, No. 4, pp. 419–427. © The Author(s), 2023. This article is an open access publication.
Russian Text © The Author(s), 2023, published in Fizika Plazmy, 2023, Vol. 49, No. 4, pp. 322–331.

TOKAMAKS

Classification of Edge Instabilities at Globus-M2 Tokamak

V. V. Solokha[a, *], G. S. Kurskiev[a], A. Yu. Yashin[a, b], I. M. Balachenkov[a], V. I. Varfolomeev[a], A. V. Voronin[a], V. K. Gusev[a], V. Yu. Goryainov[a], V. V. Dyachenko[a], N. S. Zhiltsov[a], E. O. Kiselev[a], V. B. Minaev[a], A. N. Novokhatsky[a], Yu. V. Petrov[a], A. M. Ponomarenko[b], N. V. Sakharov[a], A. Yu. Telnova[a], E. E. Tkachenko[a], V. A. Tokarev[a], S. Yu. Tolstyakov[a], E. A. Tukhmeneva[a], N. A. Khromov[a], and P. B. Shchegolev[a]

[a] *Ioffe Institute, Russian Academy of Sciences, St. Petersburg, 194021 Russia*

[b] *Peter the Great St. Petersburg Polytechnic University, St. Petersburg, 195251 Russia*

**e-mail: vsolokha@mail.ioffe.ru*

Received November 9, 2022; revised January 27, 2023; accepted January 28, 2023

Abstract—Among the peripheral instabilities observed at the Globus-M2 tokamak, two types of edge localized modes (ELMs) are brought into focus: ELMs synchronized and desynchronized with the sawtooth oscillations. The desynchronized ELMs appear in regimes that are characterized by high values of pressure in the pedestal, $p_{ped} \geq 3$ kPa, and they are observed in discharges with the toroidal magnetic field $B_T > 0.6$ T and plasma current $I_P > 0.3$ MA. The desynchronized ELMs belong to the type-III/V with the dominating effect of the peeling mode. The synchronized ELMs were observed in a wider range of discharge parameters, including at $B_T < 0.6$ T and $I_P < 0.3$ MA. Calculations of the stability of the peeling-ballooning (PB) mode showed that at pedestal width $\psi_{norm} = 0.09$ and $p_{ped} > 3.5$ kPa, destabilization of PB modes is possible without additional influence. Experimental data shows that the microtearing mode plays a dominant role in the pedestal. The microtearing mode does not allow the pedestal at Globus-M2 tokamak to reach the state of the unstable kinetic ballooning mode (KBM), which explains the low predictive power of the EPED model at this tokamak.

Keywords: high-temperature plasma, tokamak, pedestal, peeling-ballooning instability

DOI: 10.1134/S1063780X23600184

INTRODUCTION

ELMs in tokamaks [1] are a destructive and undesirable consequence of operation in the improved confinement regime [2] and they are inadmissible in the fusion reactor prototype. ELMs lead to the stochastization of magnetic field lines [3, 4] with a consequent loss of plasma ions and electrons that escape into the region of open magnetic field lines. The particles at the open field lines increase the thermal loads on the first wall of the tokamak and further cause its destruction. The destabilization of ELMs occurs under the action of the pressure gradient for the weak magnetic field side and the current flowing near the separatrix. To describe the development and burst edge instabilities, the PB mode model [5] is used and its derivative EPED model [6]. ELMs were observed in the plasma of a number of large tokamaks: JET [7], DIII-D [8], ASDEX [9], MAST [10], and NSTX [11]. They can be classified into different types; however, the most important for this study are type-I [12], type-III [12], and type-V [13] ELMs. Type-I ELMs are characterized by the increase of the frequency with raise of the input power and maximum energy loss compared to other types. Type-III and type-V ELMs develop at the same values of collisionality and lead to insignificant energy losses [14]. The difference between type-III and type-V ELMs is the reaction of the repetition rate of instability bursts to the increase of input power: for type-III, the repetition rate of bursts follows the increase of input power while for type-V, no such dependence was found. Since bursts of type-V ELMs were observed only at the NSTX spherical tokamak [13], further, we will not distinguish type-III and type-V ELMs. Earlier, it was shown that, at the Globus-M tokamak [15], ELMs do not follow the classical typification since they were observed in the improved confinement regime and with predominant (over 90% of the cases) synchronization with sawtooth oscillations. Classical ELMs were not observed, since, due to the insufficiently high plasma parameters, the pedestal (pressure profile in the peripheral region of the plasma column) did not reach the values that correspond to the destabilized PB mode. The proposed synchronization mechanism for the sawtooth oscillations and ELMs by the induced current perturbation is described in [16].

In this work, ELMs were experimentally studied in the plasma of Globus-M2 tokamak with characteristic parameters $R = 0.36$ m, $a = 0.24$ m, $B_T = 0.9$ T, and $I_P < 0.5$ MA [17], where R is the major radius, a is the minor radius, B_T is the toroidal magnetic field, and I_P is the plasma current. The Globus-M2 tokamak is a modernized version of the Globus-M tokamak ($R = 0.36$ m, $a = 0.24$ m, $B_T = 0.5$ T, and $I_P < 0.3$ MA) [18]. Due to the 80% increase in the magnetic field and, consequently, the plasma current; the energy confinement time in Globus-M2 increased threefold [19], and the confinement of fast particles also improved, which led to the changes of the pedestal parameters and, consequently, the conditions under which the PB mode develops. In this work, experimental methods of studying ELMs are described in the plasma of Globus-M2 tokamak, a classification of ELMs is proposed, and the results of numerical simulations of the PB mode are presented that are the theoretical basis of the presented classification.

The main diagnostics for the studies of ELMs was the spectrometric diagnostics of the atomic deuterium line D_α (656.3 nm) while the presence of sawtooth oscillations was detected by the soft X-ray (SXR) diagnostics. These diagnostics were used to detect the presence and synchronization of ELMs. The Doppler backscattering diagnostics (DBS) [20] was used to detect the filamentary structures and small-scale fluctuations of density (wave numbers $k_\perp = 2–13$ cm^{-1}); magnetic probes were used to estimate the relative value of the magnetic perturbation during ELMs. The magnetic configuration of the plasma was reconstructed by the method of current rings [21]. The chord-average electron density was determined by the microwave interferometry diagnostics. The temperature and electron density profiles were measured by the Thomson scattering (TS) diagnostics [22].

ANALYSIS OF EXPERIMENTAL DATA

ELMs at Globus-M2 tokamak are observed in discharges that show the signs of transition into the improved confinement regime (Fig. 1), such as the decrease of intensity of the D_α line and the increase of the chord-average plasma electron density n_e. Software processing by the dynamic time warping algorithm (DTW) [23] was used for the preliminary analysis of the database of Globus-M2 tokamak. As a result, 24 discharges were chosen. For discharges with limiter configuration, the power required for the L–H transition was 2–3 times higher than for discharges with divertor configuration [24]. Consequently, we studied only the discharges with divertor configuration and additional heating via neutral beam injection, since in these discharges, a wider range of variation of input power in the H-mode is possible. In 20 discharges out of the chosen 24, ELMs synchronized with sawtooth oscillations were observed and in 4 discharges, ELMs desynchronized with such reconnections were observed. Figure 1 shows discharge no. 41105 with desynchronized ELMs. The desynchronized ELMs are almost never (in less than 5% cases) observed at plasma currents $I_P < 0.3$ MA, yet at plasma currents $I_P > 0.3$ MA, they constitute over 50% of the total number of bursts (Fig. 2). Note that, at toroidal field $B_T < 0.6$ T, no desynchronized bursts were found, which indicates the important role of the magnetic field and, consequently, of the energy confinement time, which linearly depends on B_T and has a square root dependence on I_P [19]. Thus, the development of classical ELMs is observed in discharges with high values of $B_T > 0.6$ T and $I_P > 0.3$ MA since for such discharges, the energy confinement time $\tau_e > 5$ ms and high values of pressure are observed in the pedestal.

The synchronized and desynchronized ELMss have different dependencies of the period between bursts on the chord-average density. For ELMs synchronized with the reconnections, the period has a positive dependence on the chord-average density since the reconnection period increases with increasing n_e. When density increases, the Alfvén time decreases and, consequently, the growth rate of the kink instability also decreases [25]. An increase of the current is required to maintain the discharge stability [26] and for operation in the improved confinement regime [27], which leads to the increase of the inversion radius and, consequently, the period of sawtooth oscillations. The period of desynchronized ELMs depends only on the plasma parameters in the pedestal. The number of desynchronized ELMs increases with increasing electron density. This result is in agreement with the scaling for type-III ELMs [7] and does not contradict the type-V ELM scalings [11].

Comparison of regimes with different types of ELMs was carried out in four discharges with $B_T = 0.8$ T: nos. 40707 ($I_P = 0.21$ MA), 40715 ($I_P = 0.4$ MA), 41105 ($I_P = 0.4$ MA), and 41585 ($I_P = 0.4$ MA).

In the plasma of the Globus-M2 tokamak, the ELMs can be separated into three types depending on their synchronization with the sawtooth oscillations. The first type are ELMs completely synchronized with the reconnections (Fig. 3a). ELMs of this type are observed in discharges with plasma current and average linear density in the entire range of considered parameters (Fig. 2). The second type are ELMs that are partly synchronized with the reconnections: one synchronized burst of the edge instability followed by several (up to 3) desynchronized ELMs (Fig. 3b). The partly desynchronized ELMs are observed in discharges with high current ($I_P > 0.3$ MA) and neutral injection power $P_{NBI} = 0.4$ MW. When the input power is increased to $P_{NBI} = 0.5–0.6$ MW, the third type of ELMs appears: the completely desynchronized ELMs (Fig. 3c). At total desynchronization, synchronized

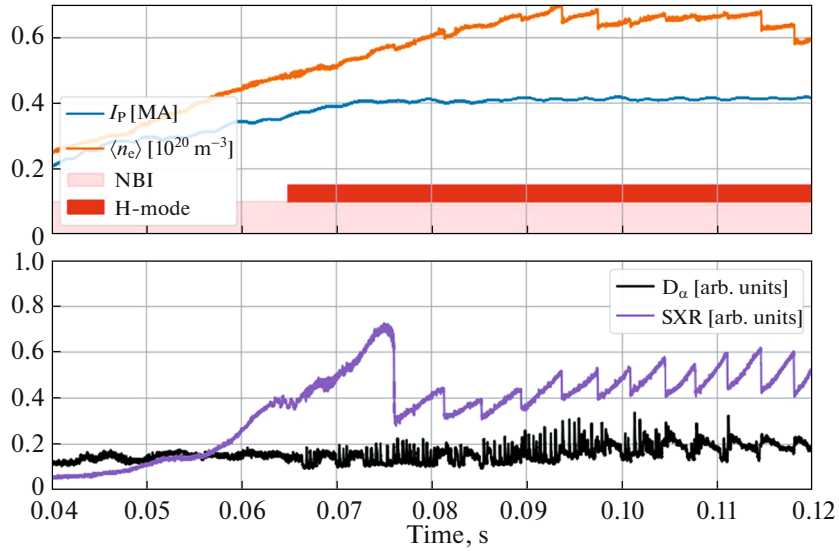

Fig. 1. Time dependences of plasma parameters in discharge no. 41105 of Globus-M2 tokamak: plasma current (blue curve), chord-average density (orange curve), radiation intensity of the D_α line (black curve), and radiation intensity of SXR radiation (purple curve). The rectangles show the time intervals during which the plasma was heated by the beam of neutral particles with $P_{NBI} \approx 0.5$ MW (pink rectangle) and when it was in the improved confinement regime (red rectangle).

ELMs do not disappear, but they become statistically less important because for one synchronized burst, 6 and more desynchronized ELMs are observed (Fig. 2). Increasing the additional heating power does not affect the frequency of desynchronized ELMs. In discharge no. 41585 with desynchronized ELMs, the input power of additional heating was varied from $P_{NBI} = 0.5$ MW to $P_{NBI} = 0.8$ MW (Fig. 4), and the ELM frequency did not change, which, together with the measured direct dependence of the ELM frequency on the chord-average density and the temperature near the separatrix $T_e = 300$ eV typical for type-III ELMs [28] allows one to conclude that type-III/V ELMs are present with a dominant effect of the peeling mode.

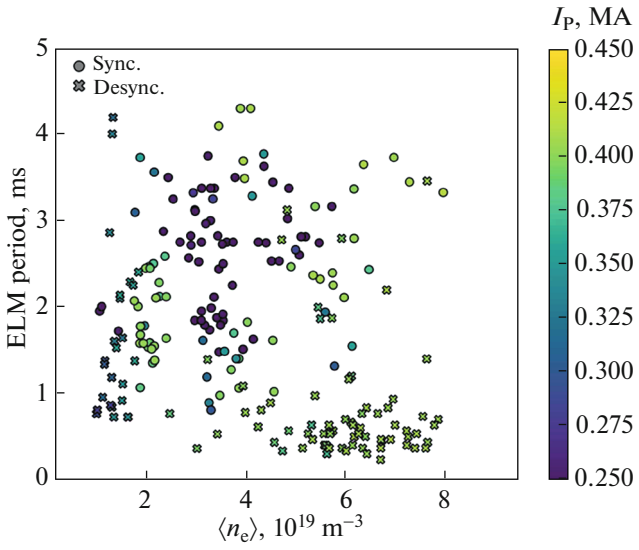

Fig. 2. Dependence of the period between bursts of the edge instability on the chord-average density (x-axis) and plasma current (color scale). Circles mark ELMs synchronized with reconnections and crosses mark ELMs desynchronized with reconnections.

The electron density and temperature profiles obtained by the TS diagnostics show that discharges with partially synchronized ELMs have a 60% higher pressure in the pedestal than discharges with synchronized ELMs, $p_{ped} = 2.5$ kPa and $p_{ped} = 1.5$ kPa, respectively. These discharges show close values of electron density n_e (the difference being <20%), yet the electron temperature in the case with partially desynchronized bursts of edge instabilities is 1.5 times higher (Fig. 5). Discharges with completely desynchronized ELMs have a pressure in the pedestal that is 50% higher ($p_{ped} = 4.0$ kPa) than in discharges with partially desynchronized ELMs and, consequently, under their conditions the PB mode can destabilize regardless of the internal reconnections. Discharges nos. 40715 ($P_{NBI} = 0.4$ MW) and 41105 ($P_{NBI} = 0.6$ MW) have the same electron temperature despite the 1.5 time increase of the input power. At identical electron temperature profiles, the electron density profile n_e in the discharges with completely synchronized ELMs is 2 times higher than in discharges with partially synchronized ELMs.

The spectrogram of the magnetic probe signals and the time dependence of the D_α radiation (Fig. 6) in

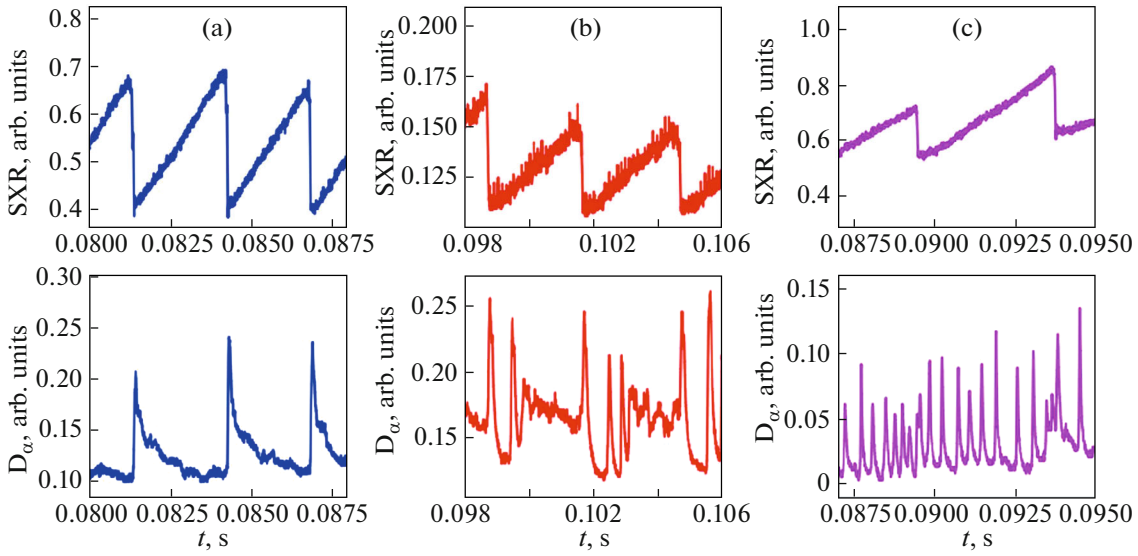

Fig. 3. (Upper row) SXR radiation intensity and (lower row) D_α radiation intensity in discharge nos. (a) 40707 with synchronized ELMs, (b) 40715 with partially desynchronized ELMs, and (c) 41105 completely desynchronized ELMs.

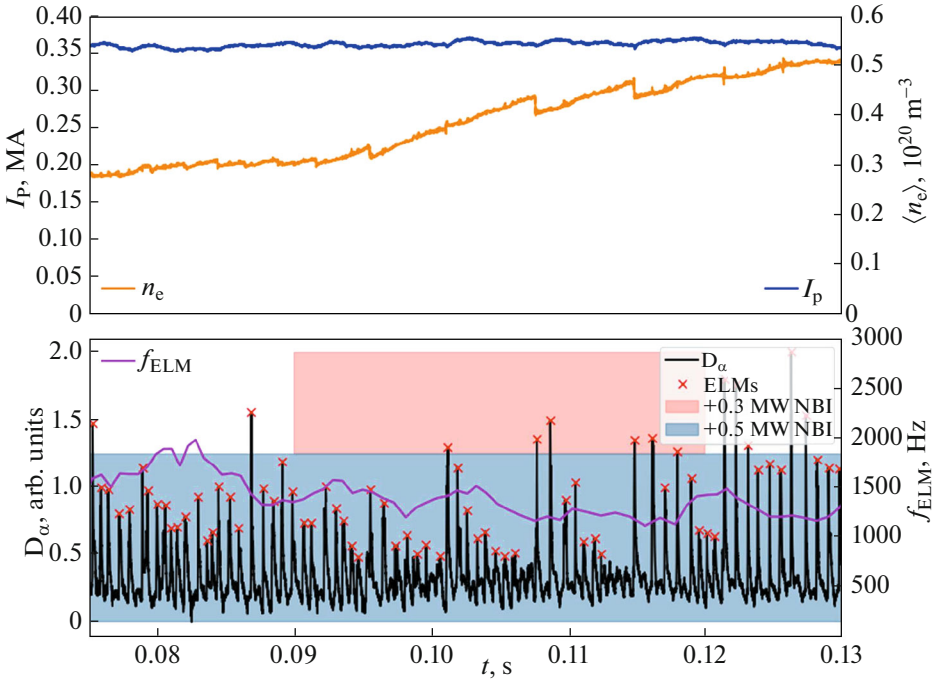

Fig. 4. Time dependences of plasma parameters in discharge no. 41585 of the Globus-M2 tokamak: plasma current (blue curve), chord-average plasma density (orange curve), D_α line radiation intensity (black curve), and the frequency of edge instability bursts (purple curve). The rectangles mark the time intervals during which the plasma was heated by the beam of neutral particles with input power of 0.5 MW (blue rectangle) and 0.3 MW (red rectangle).

discharge no. 41105 show that the magnetic perturbations during the synchronized ELMs are longer (t = 0.0895 s), however, the analysis of the data of the thermal camera shows a more substantial heating of the divertor plates in the case of desynchronized ELMs. During the improved confinement regime, the magnetic probe diagnostics recorded oscillations at the frequency of about 80 kHz, which can be the consequence of the development of the microtearing mode (MTM) with poloidal/toroidal numbers m/n = 10/2

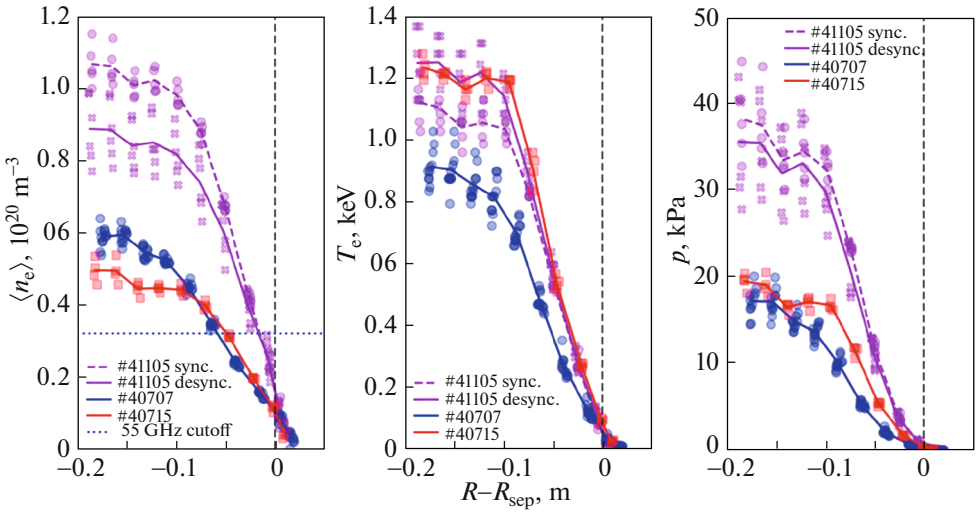

Fig. 5. Profiles of (left panel) electron density, (central panel) electron temperature, and (right panel) total pressure obtained by the TR diagnostics in discharges with synchronized ELMs (discharge no. 40707, blue curve, circles, solid line), partially desynchronized ELMs (discharge no. 40715, red curve, squares, solid curve), and no. 41105 (purple curve) in phase with partially desynchronized ELMs (crosses, solid line) and in phase with partially desynchronized ELMs (circles, dashed curve). The vertical dashed line indicates the position of the separatrix. The horizontal dotted line in the left panel indicates the position of the DBS cutoff in discharge no. 41105.

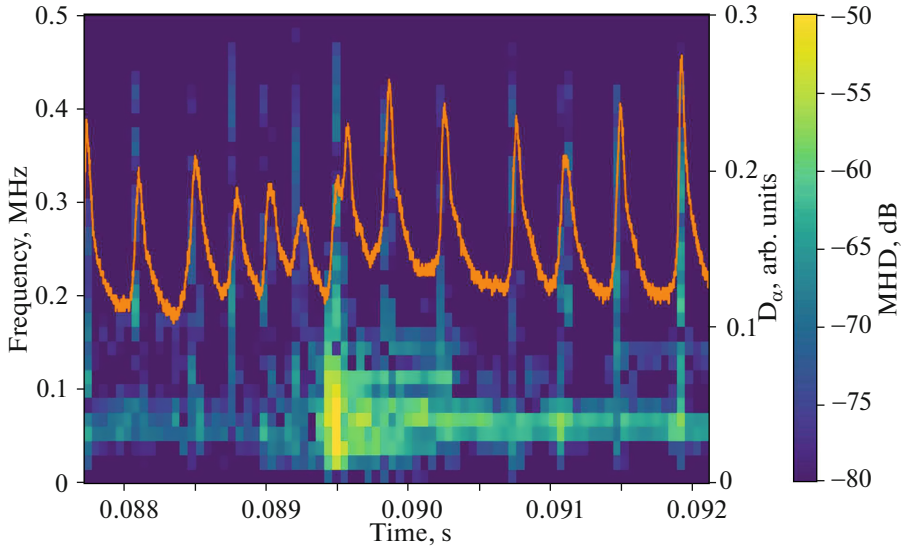

Fig. 6. Spectrogram of the magnetic probe data and intensity of radiation of the D_α line (orange) in discharge no. 41105.

[29]. Presumably, it is the development of MTM in the plasma that limits the maximum achievable value of the electron temperature T_e [30] in discharges with $P_{NBI} > 0.5$ MW. Unfortunately, studies of particle transfer and energy are outside the scope of this work.

Analysis of DBS data showed that after transition to the improved confinement regime in discharge no. 41105, the level of velocity fluctuations in the edge plasma ($R = 0.57$ m) dropped 5 times relative to their initial level (Fig. 7). The drop of the fluctuations level leads to the change of ELMs type. During the discharge (at $t = 0.105$ s), a spontaneous increase of carbon concentration occurred due to, presumably, intrusion of dust, which had an effect on both the intensity of small-scale turbulence (its intensity increased 2 times) and type of ELMs: desynchronized ELMs became partially synchronized. At the same time, the parameters of the edge plasma remained the

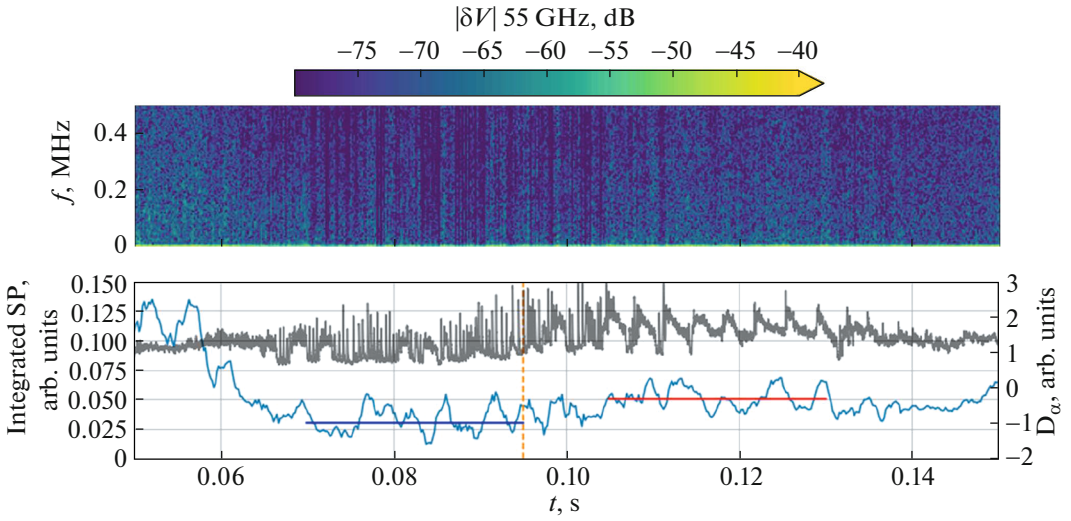

Fig. 7. (Upper panel) spectrogram of velocity fluctuations in discharge no. 41105 measured by DBS at frequency of 55 GHz and (lower panel) integrated spectral power of DBS signal in the range 0.05–1.00 MHz (blue curve) and intensity of radiation of the D_α line (black curve). The orange dashed line marks the time at which carbon intruded into the plasma with the subsequent transition from the regime of desynchronized ELMs into the regime of synchronized ELMs. The horizontal blue line marks the fluctuation level in the regime of desynchronized ELMs while the horizontal red line marks the fluctuation level in the regime of synchronized ELMs.

same. Earlier simulations [31] showed that the intrusion of impurities in the edge plasma causes the decrease of the bootstrap current. Consequently, for ELMs with the dominating effect of the peeling mode, the decrease of current density near the separatrix by 30–50% can stabilize the PB mode.

SIMULATIONS OF THE DEVELOPMENT OF THE PB MODE

To determine the qualitative characteristics of the radial plasma pressure profile (its "height" and "width") that are required for the destabilization of the PB mode regardless of the internal reconnections, simulations of PB mode stability were carried out by the BOUT++ code [32]. The set of equations of one-fluid magnetohydrodynamics (MHD) was solved by the finite difference method in the three-dimensional tokamak geometry.

In the poloidal cross section, a mesh with four-angled cells was used that was based on magnetic surfaces. The mesh had a 64 × 32 resolution and coverage $\psi_{norm} = 0.70–0.97$. It was built using the magnetic equilibrium EFIT data for discharge no. 40707 with elongation $\varepsilon = 1.83$ and average triangularity $\delta = 0.35$ [33]. The toroidal mode numbers were limited by $n < 45$. Simulations were carried out with time step equal to 0.5 Alfvén times (τ_A). The initial plasma pressure profile had the shape of hyperbolic tangent and it was given by two parameters, its width and its height. The current density profile consisted of the Ohmic and bootstrap components. The Ohmic component was assumed to be constant within the mesh and it was taken from simulations by the ASTRA code for similar discharges. The bootstrap component was calculated by the formula derived in [31]. The pressure of fast ions p_{fast} relative to the total plasma pressure p_{total} in Globus-M2 discharges does not exceed $p_{fast}/p_{total} < 0.1$ and it can be neglected.

To analyze the pedestal stability, a stability diagram was constructed (Fig. 8), which depicts the dependence of the growth rate of PB instability on the width and height of the pedestal. To construct the diagram, root-mean-square perturbations of pressure were calculated in each point of the pedestal height and width. In the poloidal cross section, a position was chosen of the equatorial plane from the weak magnetic field side, at which the instability growth rate was calculated from the root-mean-square pressure perturbation, and it was ascribed to these pedestal parameters. In the case of completely synchronized ELMs, the pedestal was in the stable region and, consequently, the PB mode could not destabilize in the absence of an additional current perturbation. In discharges with partly synchronized ELMs, the pedestal parameters were at the boundary of the stable region and, consequently, for the PB mode to destabilize, a current perturbation was required after which several additional instability cycles were observed. The pedestal parameters in discharges with completely desynchronized ELMs were in the strongly unstable region and therefore, they did not require current perturbations for the PB mode to destabilize. For discharge parameters with completely destabilized ELMs, the most unstable modes had mode numbers $n = 4–6$, which correspond to type-III or type-V ELMs.

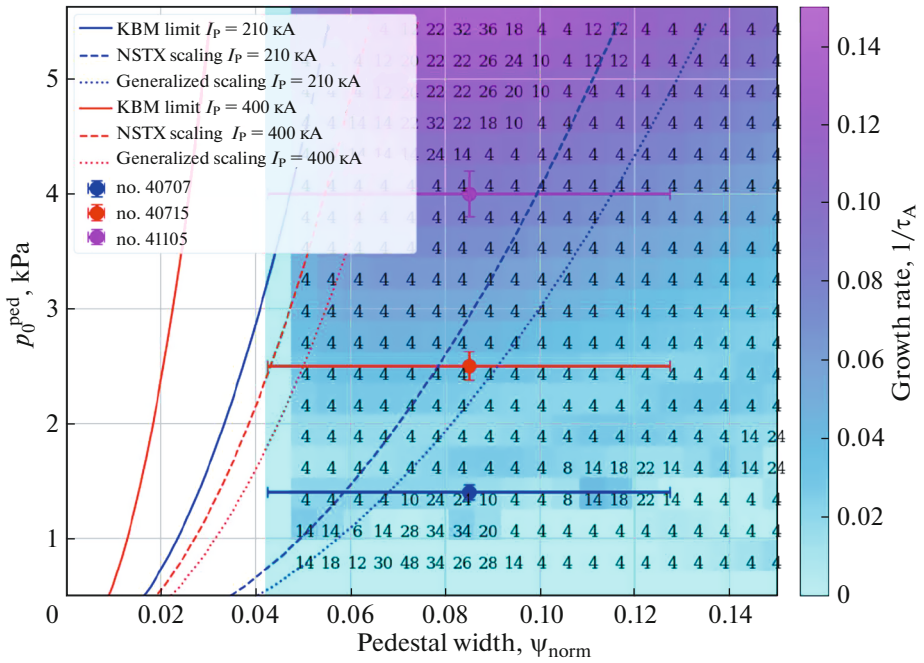

Fig. 8. Growth rate of the peeling-ballooning instability and the toroidal number of the most unstable mode; experimental values of pressure in the pedestal (points), the limiting width of the pedestal with KBM $\Delta = 0.089\sqrt{\beta_{p,\mathrm{ped}}}$ (solid curves); the limiting width of the pedestal by the NSTX scaling (dashed curves), and the limiting width of the pedestal by the generalized scaling (dotted curves).

Analysis of the predicted height and width of the pedestal by the EPED model [6] for type-I ELM showed that, in its current state, the model is not applicable to the Globus-M2 plasma. The main criterion of the applicability of the EPED model is the condition for the presence of the destabilized kinetic ballooning mode (KBM) in the pedestal. This condition connects the height and width of the pedestal with the criterion $\Delta = 0.089\sqrt{\beta_{p,\mathrm{ped}}}$, where Δ is the pedestal width and $\beta_{p,\mathrm{ped}}$ is the poloidal beta at the top of the pedestal. Nevertheless, KBM is stable according to the approximation of the critical ballooning pedestal in the entire region of the stable PB mode since the experimental values of the pedestal width are much higher than those that are required for the condition of the destabilized KBM (Fig. 8). The MTM, which also can limit the height and width of the pedestal, develops at lower pressure gradients and it is characteristic of spherical tokamaks [34]. Consequently, the width and height of the pedestal that does not satisfy the KBM limitation as well as the experimental proof of the development of MTM demonstrate the key role of MTM in limiting the pedestal parameters. At the same time, the scaling for the NSTX spherical tokamak [35] shows a better agreement with the experimental values obtained at the Globus-M2 tokamak. Yet it is the generalized scaling for the pedestal width [36, 37] that provides values that agree with experimental results obtained at Globus-M2. This shows that the EPED model is inapplicable to the pedestal of Globus-M2 tokamak and needs to be modernized before its usage for spherical tokamaks.

CONCLUSIONS

In Globus-M2 tokamak, ELMs that are synchronized and desynchronized with internal reconnections (sawtooth oscillations) are observed. Desynchronized ELMs are type-III/V ELMs with a dominating effect of the peeling mode, and they develop at high values of the plasma current, toroidal magnetic field, and neutral beam injection power ($I_P > 0.3$ MA, $B_T > 0.6$ T, and $P_{NBI} > 0.5$ MW, respectively). Their development requires pressure in the pedestal $p_{ped} > 3.5$ kPa, which destabilizes the PB mode. Pedestals with such high pressures are possible in the improved confinement regime, when the intensity of small-scale fluctuations decreases 5-fold relative to their level that corresponds to the L–H transition. A key role in reaching the required pressure is played by gas puffing since at the Globus-M2 tokamak, the increase of electron temperature when the input power is increased is limited by the development of the MTM and the only method of increasing the pressure in the pedestal is increasing the electron density.

ACKNOWLEDGMENTS

The experiments were carried out at the Unique Scientific Installation "Globus-M Spherical Tokamak," which is a part of the Federal Center for the Collective Use of Scientific Equipment "Materials Science and Diagnostics in Advanced Technologies."

FUNDING

The measurement of spatial distributions of electron temperature, presented in the section "Analysis of Experimental Data," was carried out within the framework of the State Assignment no. 0040-2019-0023. The experiments on plasma heating by neutral injection, presented in the section "Analysis of Experimental Data," were carried out within the framework of the State Assignment no. 0034-2021-0001. The simulation of MHD-stability and measurements of plasma rotation velocity fluctuations using DBS diagnostics, presented in the section "Simulation of the Development of the PB Mode," were supported by the Russian Science Foundation, grant no. 18-72-10028.

CONFLICT OF INTEREST

The authors declare that they have no conflicts of interest.

REFERENCES

1. A. W. Leonard, Phys. Plasmas **21**, 090501 (2014). https://doi.org/10.1063/1.4894742
2. F. Wagner, G. Fussmann, T. Grave, M. Keilhacker, M. Kornherr, K. Lackner, K. McCormick, E. R. Muller, A. Stäbler, G. Becker, K. Bernhardi, U. Ditte, A. Eberhagen, O. Gehre, J. Gernhardt, et al., Phys. Rev. Lett. **53**, 1453 (1984). https://doi.org/10.1103/PhysRevLett.53.1453
3. H. R. Wilson and S. C. Cowley, Phys. Rev. Lett. **92**, 175006 (2004). https://doi.org/10.1103/PhysRevLett.92.175006
4. M. Lampert, A. Diallo, J. R. Myra, and S. J. Zweben, Phys. Plasmas **28**, 022304 (2021). https://doi.org/10.1063/5.0031322
5. P. B. Snyder, H. R. Wilson, J. R. Ferron, L. L. Lao, A. W. Leonard, T. H. Osborne, A. D. Turnbull, D. Mossessian, M. Murakami, and X. Q. Xu, Phys. Plasmas **9**, 2037 (2002). https://doi.org/10.1063/1.1449463
6. P. B. Snyder, R. J. Groebner, J. W. Hughes, T. H. Osborne, M. Beurskens, A. W. Leonard, H. R. Wilson, and X. Q. Xu, Nucl. Fusion **51**, 103016 (2011). https://doi.org/10.1088/0029-5515/51/10/103016
7. A. Loarte, M. Becoulet, G. Saibene, R. Sartori, D. J. Campbell, T. Eich, A. Herrmann, M. Laux, W. Suttrop, B. Alper, P. J. Lomas, G. Matthews, S. Jachmich, J. Ongena, P. Innocente, et al., Plasma Phys. Controlled Fusion **44**, 1815 (2022). https://doi.org/10.1088/0741-3335/44/9/303
8. H. Zohm, T. H. Osborne, K. H. Burrell, M. S. Chu, E. J. Doyle, P. Gohil, D. N. Hill, L. L. Lao, A. W. Leonard, T. S. Taylor, and A. D. Turnbull, Nucl. Fusion **35**, 543 (1995). https://doi.org/10.1088/0029-5515/35/5/I05
9. T. Kass, S. Günter, M. Maraschek, W. Suttrop, H. Zohm, and ASDEX Upgrade Team, Nucl. Fusion **38**, 111 (1998). https://doi.org/10.1088/0029-5515/38/1/310
10. S. Saarelma, T. C. Hender, A. Kirk, H. Meyer, H. R. Wilson, and MAST Team, Plasma Phys. Controlled Fusion **49**, 31 (2007). https://doi.org/10.1088/0741-3335/49/1/003
11. R. Maingi, C. E. Bush, E. D. Fredrickson, D. A. Gates, S. M. Kaye, B. P. LeBlanc, J. E. Menard, H. Meyer, D. Mueller, N. Nishino, A. L. Roquemore, S. A. Sabbagh, K. Tritz, S. J. Zweben, M. G. Bell, et al., Nucl. Fusion **45**, 1066 (2005). https://doi.org/10.1088/0029-5515/45/9/006
12. H. Zohm, Plasma Phys. Controlled Fusion **38**, 105 (1996). https://doi.org/10.1088/0741-3335/38/2/001
13. R. Maingi, M. G. Bell, E. D. Fredrickson, K. C. Lee, R. J. Maqueda, P. Snyder, K. Tritz, S. J. Zweben, R. E. Bell, T. M. Biewer, C. E. Bush, J. Boedo, N. H. Brooks, L. Delgado-Aparicio, C. W. Domier, et al., Phys. Plasmas **13**, 092510 (2006). https://doi.org/10.1063/1.2226986
14. P. T. Lang, A. Loarte, G. Saibene, L. R. Baylor, M. Becoulet, M. Cavinato, S. Clement-Lorenzo, E. Daly, T. E. Evans, M. E. Fenstermacher, Y. Gribov, L. D. Horton, C. Lowry, Y. Martin, O. Neubauer, et al., Nucl. Fusion **53**, 043004 (2013). https://doi.org/10.1088/0029-5515/53/4/043004
15. V. V. Solokha, G. S. Kurskiev, V. V. Bulanin, A. V. Petrov, S. Yu. Tolstyakov, E. E. Mukhin, V. K. Gusev, Yu. V. Petrov, N. V. Sakharov, V. A. Tokarev, N. A. Khromov, M. I. Patrov, N. N. Bakharev, A. D. Sladkomedova, A. Yu. Telnova, et al., J. Phys.: Conf. Ser. **1094**, 012002 (2018). https://doi.org/10.1088/1742-6596/1094/1/012002
16. V. V. Bulanin, G. S. Kurskiev, V. V. Solokha, A. Yu. Yashin, and N. S. Zhiltsov, Plasma Phys. Controlled Fusion **63**, 122001 (2021). https://doi.org/10.1088/1361-6587/ac36a4
17. V. B. Minaev, V. K. Gusev, N. V. Sakharov, V. I. Varfolomeev, N. N. Bakharev, V. A. Belyakov, E. N. Bon-

darchuk, P. N. Brunkov, F. V. Chernyshev, V. I. Davydenko, V. V. Dyachenko, A. A. Kavin, S. A. Khitrov, N. A. Khromov, E. O. Kiselev, et al., Nucl. Fusion **57**, 066047 (2017). https://doi.org/10.1088/1741-4326/aa69e0

18. V. K. Gusev, V. E. Golant, E. Z. Gusakov, V. V. D'yachenko, M. A. Irzak, V. B. Minaev, E. E. Mukhin, A. N. Novokhatskii, K. A. Podushnikova, G. T. Razdobarin, N. V. Sakharov, E. N. Tregubova, V. S. Uzlov, O. N. Shcherbinin, V. A. Belyakov, et al., Tech. Phys. **44**, 1054 (1999). https://doi.org/10.1134/1.1259469
19. G. S. Kurskiev, V. K. Gusev, N. V. Sakharov, Yu. V. Petrov, N. N. Bakharev, I. M. Balachenkov, A. N. Bazhenov, F. V. Chernyshev, N. A. Khromov, E. O. Kiselev, S. V. Krikunov, V. B. Minaev, I. V. Miroshnikov, A. N. Novokhatskii, N. S. Zhiltsov, et al., Nucl. Fusion **62**, 016011 (2022). https://doi.org/10.1088/1741-4326/ac38c9
20. A. Yashin, V. Bulanin, A. Petrov, and A. Ponomarenko, Appl. Sci. **11**, 8975 (2021). https://doi.org/10.3390/app11198975
21. N. V. Sakharov, A. V. Voronin, V. K. Gusev, A. A. Kavin, S. N. Kamenshchikov, K. M. Lobanov, V. B. Minaev, A. N. Novokhatsky, M. I. Patrov, Yu. V. Petrov, and P. B. Shchegolev, Plasma Phys. Rep. **41**, 997 (2015). https://doi.org/10.1134/S1063780X15120120
22. G. S. Kurskiev, N. S. Zhil'tsov, A. N. Koval', A. F. Kornev, A. M. Makarov, E. E. Mukhin, Yu. V. Petrov, N. V. Sakharov, V. A. Solovei, E. E. Tkachenko, S. Yu. Tolstyakov, and P. V. Chernakov, Pis'ma Zh. Tekh. Fiz. **47** (24), 41 (2021). https://doi.org/10.21883/PJTF.2021.24.51799.19019
23. M. Müller, *Information Retrieval for Music and Motion* (Springer, Berlin, 2007), p. 69. https://doi.org/10.1007/978-3-540-74048-3_4
24. D. Kalupin, M. Z. Tokar, B. Unterberg, X. Loozen, D. Pilipenko, R. Zagorski, and TEXTOR Contributors, Plasma Phys. Controlled Fusion **48**, A309 (2006). https://doi.org/10.1088/0741-3335/48/5A/S30
25. F. Porcelli, D. Boucher, and M. N. Rosenbluth, Plasma Phys. Controlled Fusion **38**, 2163 (1996). https://doi.org/10.1088/0741-3335/38/12/010
26. M. Greenwald, J. L. Terry, S. M. Wolfe, S. Ejima, M. G. Bell, S. M. Kaye, and G. H. Neilson, Nucl. Fusion **28**, 2199 (1988). https://doi.org/10.1088/0029-5515/28/12/009
27. T. Eich, R. J. Goldston, A. Kallenbach, B. Sieglin, H. J. Sun, ASDEX Upgrade Team, and JET Contributors, Nucl. Fusion **58**, 034001 (2018). https://doi.org/10.1088/1741-4326/aaa340
28. W. Suttrop, M. Kaufmann, H. J. de Blank, B. Brüsehaber, K. Lackner, V. Mertens, H. Murmann, J. Neuhauser, F. Ryter, H. Salzmann, J. Schweinzer, J. Stober, H. Zohm, and the ASDEX Upgrade Team, Plasma Phys. Controlled Fusion **39**, 2051 (1997). https://doi.org/10.1088/0741-3335/39/12/008
29. J. L. Larakers, M. Curie, D. R. Hatch, R. D. Hazeltine, and S. M. Mahajan, Phys. Rev. Lett. **126**, 225001 (2021). https://doi.org/10.1103/PhysRevLett.126.225001
30. A. O. Nelson, F. M. Laggner, A. Diallo, D. Smith, Z. A. Xing, R. Shousha, and E. Kolemen, Nucl. Fusion **61**, 116038 (2021). https://doi.org/10.1088/1741-4326/ac27ca
31. A. Redl, C. Angioni, E. Belli, O. Sauter, ASDEX Upgrade Team, and EUROfusion MST1 Team, Phys. Plasmas **28**, 022502 (2021). https://doi.org/10.1063/5.0012664
32. B. D. Dudson, M. V. Umansky, X. Q. Xu, P. B. Snyder, and H. R. Wilson, Comput. Phys. Commun. **180**, 1467 (2009). https://doi.org/10.1016/j.cpc.2009.03.008
33. L. L. Lao, H. E. St. John, Q. Peng, J. R. Ferron, E. J. Strait, T. S. Taylor, W. H. Meyer, C. Zhang, and K. I. You, Fusion Sci. Technol. **48**, 968 (2005). https://doi.org/10.13182/FST48-968
34. D. Dickinson, C. M. Roach, S. Saarelma, R. Scannell, A. Kirk, and H. R. Wilson, Phys. Rev. Lett. **108**, 135002 (2012). https://doi.org/10.1103/PhysRevLett.108.135002
35. A. Diallo, R. Maingi, S. Kubota, A. Sontag, T. Osborne, M. Podesta, R. E. Bell, B. P. LeBlanc, J. Menard, and S. Sabbagh, Nucl. Fusion **51**, 103031 (2011). https://doi.org/10.1088/0029-5515/51/10/103031
36. S. Yu. Medvedev, A. A. Ivanov, A. A. Martynov, Yu. Yu. Poshekhonov, S. V. Konovalov, and A. R. Polevoi, Plasma Phys. Rep. **42**, 472 (2016). https://doi.org/10.1134/S1063780X1605010X
37. S. Yu. Medvedev, A. A. Martynov, S. V. Konovalov, V. M. Leonov, V. E. Lukash, and R. R. Khairutdinov, Plasma Phys. Rep. **47**, 1119 (2021). https://doi.org/10.1134/S1063780X21110222

Translated by E. Voronova